



## Abstract

Injection of basaltic magmas into silicic crustal holding chambers and subsequent mixing of the two components is a process that has been recognised since the late seventies to have resulted in explosive eruptions. Detailed reconstruction and assessment of the mixing process caused by such intrusion is now possible because of the exceptional time-sequence sample suite available from the tephra fallout of the 2010 summit eruption at Eyjafjallajökull volcano in South Iceland. From 14 to 19 April the tephra contains three glass types of basaltic, intermediate, and silicic compositions recording rapid magma mingling without homogenisation, involving evolved FeTi-basalt and dacite with composition identical to that produced by the 1821–1823 AD Eyjafjallajökull summit eruption. The time-dependent change in the magma composition suggests a binary mixing process with changing end-member compositions and proportions, or dynamic magma mixing. Beginning of May, a new injection of deep-derived basalt was recorded by deep seismicity, appearance of magnesium-rich olivine phenocrysts together with high sulphur output and presence of sulphide crystals. Thus the composition of the basaltic injection became more primitive and hotter with time provoking changes in the silicic mixing end-member from pre-existing melt to the solid carapace of the magma chamber. Decreasing proportions of the mafic end-member with time in the erupted mixed-magma, demonstrate that injections of Mg-rich basalt was the motor of the 2010 Eyjafjallajökull explosive eruption, and that its decreasing inflow terminated the eruption. Significant quantity of silicic magma is thus still present in the interior of the volcano. Our results show that detailed sampling during the entire eruption was essential for deciphering the complex magmatic processes at play, namely the dynamic magma mixing. Finally, the rapid compositional changes in the eruptive products suggest that magma mingling occurs on a timescale of few hours to days whereas the interval between the first detected magma injection and eruption was several months.

## Dynamic magma mixing

O. Sigmarsson et al.

Title Page

Abstract

Introduction

Conclusions

References

Tables

Figures

◀

▶

◀

▶

Back

Close

Full Screen / Esc

Printer-friendly Version

Interactive Discussion



## 1 Introduction

Improved understanding of volcanic plumbing-systems is needed for better interpretations of precursors for volcanic eruptions. While deformation and seismic studies yield real-time information of physical changes beneath a volcano, geochemical investigation of the eruptive products allows identification of magma source and quantification of magmatic processes leading to an eruption. Here, we use petrological and geochemical evidences, obtained on a precisely dated sample-suite of lava and tephra from the 2010 Eyjafjallajökull eruption in south Iceland (Fig. 1), to evaluate the triggering mechanism for the 2010 summit eruption and to quantify the magma differentiation processes. We show that basaltic injection remobilized older silicic magma causing explosive eruption of inhomogeneous mixture of mingled magma. We also demonstrate how fast the composition and proportions of the mixing end-members changed, or the dynamics of magma mixing.

## 2 The Eyjafjallajökull 2010 eruption

Over the last fifteen years, episodic seismic swarms and inflation-induced deformation have been taken to indicate sill injections at mid-crustal depth beneath Eyjafjallajökull volcano (Gudmundsson et al., 2010; Sigmundsson et al., 2010). A deep-sourced inflation started December 2009 accompanied by decreasing depth of seismicity. Deformation and earthquake activity continued until late 20 March 2010 when a flank eruption broke out on a radial fissure at the Fimmvörðuháls Pass, between Eyjafjallajökull and Mýrdalsjökull ice-caps (Fig. 1). The eruption produced olivine- and plagioclase-phyric primitive and relatively homogeneous mildly-alkaline basalt until 12 April (Fig. 2). This was followed by a seismic swarm that migrated rapidly from depth of more than 5 km towards the summit of the volcano (Hjaltadóttir et al., 2011) culminating in an explosive eruption in the early morning on 14 April. Magma-water interaction was intensive during the first two days but gradually declined, and the activity became purely magmatic by 21 April. During the first six days magma discharge was on the order of  $10^6 \text{ kg s}^{-1}$ ,

SED

3, 591–613, 2011

### Dynamic magma mixing

O. Sigmarrsson et al.

Title Page

Abstract

Introduction

Conclusions

References

Tables

Figures

◀

▶

◀

▶

Back

Close

Full Screen / Esc

Printer-friendly Version

Interactive Discussion



dropped to  $10^4$ – $10^5$  kg s<sup>-1</sup> until early May when activity picked up and reached a discharge of  $10^5$  kg s<sup>-1</sup> again on 5–6 May, followed by an irregular decline in discharge until the end of the eruption late May. The magma produced is of a benmoritic to trachytic composition with very fine to fine ash that disturbed air-traffic over Europe for extended periods in April and May.

### 3 Samples

Our sample suite is comprised of basaltic lava (FH-1) and tephra (FH-2) from the initial phase of the flank eruption at Fimmvörðuháls, a tephra (FH-3) collected directly from the fallout from the plume on 1 April, and lava (FH-4) from the last stage of the eruption. The benmoritic sample suite includes tephra collected 15 April (EJ-1), a composite sample of tephra produced 17–19 April (EJ-2), and tephra from 22 April (EJ-3), 27 April (EJ-4), and 5 May tephra (EJ-5), in addition to two bread-crust bombs of trachyte composition (EJ-6,7) from the final days of the eruption, collected on 3 June 2010 from the surface of 45 m thick tephra pile on the eastern rim of the new crater. Tephra from the 1821–1823 penultimate eruption of Eyjafjallajökull was sampled from a soil section on the western flank of the volcano for comparison. The exact timing of our samples is fundamental for precisely deciphering the magma dynamics prior to and during the eruption.

### 4 Methods

#### 4.1 Microanalytical techniques

##### 4.1.1 Electron probe microanalyses

Major element compositions of crystals and glasses were determined on Cameca SX100 electron microprobe at the Laboratoire Magmas et Volcans in Clermont-Ferrand. Operating conditions were 15 kV accelerating voltage and 15 nA focused beam for minerals. Synthetic and natural minerals standards were used for

SED

3, 591–613, 2011

## Dynamic magma mixing

O. Sigmarsson et al.

Title Page

Abstract

Introduction

Conclusions

References

Tables

Figures

◀

▶

◀

▶

Back

Close

Full Screen / Esc

Printer-friendly Version

Interactive Discussion



calibration with counting time set at 10 s for all elements. During glass analyses, analytical conditions were adjusted to minimise sodium mobility; basaltic and intermediate tephra were analysed at 4 nA and 2 nA beam current, respectively, with a 10  $\mu\text{m}$  defocused beam. Optimized mixture of minerals standards (synthetic and natural) and glasses (A-THO and VG2) was used for calibration. The counting time was 10 s for Na, Si, Ca, Ti and P; 20 s for Al and Mg; 30 s for Mn and 40 s for K and Fe. Secondary international glass standard USGS VG A-99 (Jarosewich et al., 1979; Thornber et al., 2002) was analysed during each session to monitor possible instrumental drift. Analyses during three days in a row, yield relative standard deviation of 0.6 % for  $\text{SiO}_2$ , 1–2 % for  $\text{TiO}_2$ ,  $\text{Al}_2\text{O}_3$  and CaO, 2.2 % for FeO, 3.3 % for  $\text{Na}_2\text{O}$  and  $\text{K}_2\text{O}$ , using a single set of calibration values.

#### 4.1.2 Laser ablation inductively coupled plasma mass spectrometry

Trace element analyses in glasses were performed at the Laboratoire Magmas et Volcans (Clermont-Ferrand) using a Resonetics M50 EXCIMER laser (193 nm) coupled to an Agilent 7500 cs ICP-MS. The laser was operated at 6 mJ energy, 2 Hz repetition rate and a 11  $\mu\text{m}$  spot size diameter. Ablation gas was pure helium; nitrogen (7 ml  $\text{min}^{-1}$ ) and argon was mixed with the carrier gas via Y-connectors between the ablation cell and ICP-MS. Analysis duration was split up in two distinct parts: 40 s background acquisition followed by 50 s data acquisition from the sample. Stability of signal intensity during ablation proved a good indicator of the analytical spot homogeneity.

The raw analyses were reduced with the Glitter software (van Achterberg et al., 2001) using CaO concentrations (measured earlier by electron microprobe) as internal standard. NIST 612 glass was used as the primary standard; NIST 610, BCR2-G and A-THO, periodically analyzed during the laser sessions, were used as reference materials for run quality control. The two latter reference glasses have similar composition as the analyzed sample and are therefore well suited to estimate precision and accuracy. Despite the small spot size, precision and accuracy were always better than 10 % for all the elements at 95 % confidence level.

## Dynamic magma mixing

O. Sigmarsson et al.

Title Page

Abstract

Introduction

Conclusions

References

Tables

Figures

◀

▶

◀

▶

Back

Close

Full Screen / Esc

Printer-friendly Version

Interactive Discussion



## 4.2 Whole-rock analysis

### 4.2.1 Major- and trace element concentrations

About 100 mg of powder sample were fluxed with lithium metaborate (proportions 1:3) in a carbon crucible using induction furnace. The melt-pearl was immediately dissolved in diluted nitric acid and diluted 2000 times before ICP-AES analysis. Another 100 mg powder aliquot was dissolved in concentrated HF-HNO<sub>3</sub>, evaporated to near dryness and re-dissolved in 7M HNO<sub>3</sub>. The aliquot was evaporated to near dryness and subsequently diluted in HNO<sub>3</sub> 0.4 M to reach a total dilution factor of 5000 for determination of trace element abundances by quadrupole ICP-MS (Agilent 7500, Laboratoire Magmas et Volcans). The reaction cell (He mode) was used to reduce interferences on masses ranging from 45 (Sc) to 75 (As). The signal was calibrated externally with a reference basaltic standard (BHVO-2, batch 759) dissolved as samples, and employing the GeoReM preferred values (<http://georem.mpch-mainz.gwdg.de/>). Both standards and pure HNO<sub>3</sub> 0.4 M were measured every 4 samples. The external reproducibility of the method, as estimated by running repeatedly different standards (BCR-2, BIR, BEN) is <5% (2σ) for most lithophile elements and <15% for chalcophile elements.

### 4.2.2 Oxygen isotopes

Laser fluorination oxygen isotope analyses were performed at the University of Oregon stable isotope laboratory using a 35 W CO<sub>2</sub>-laser. Individual grains, bulk monomineralic fractions, and glasses ranging in weight from 1.1 to 2 mg were reacted with purified BrF<sub>5</sub> reagent to liberate oxygen. The gases generated in the laser chamber were purified through a series of cryogenic traps held at liquid nitrogen temperature and a mercury diffusion pump to eliminate traces of fluorine gas. Oxygen was converted to CO<sub>2</sub> gas using a small platinum-graphite converter, and then the CO<sub>2</sub> gas was analyzed on a MAT 253 mass spectrometer integrated to the laser line. Five aliquots of standards were analyzed together with the unknown samples; Gore Mt Garnet ( $\delta^{18}\text{O} = 5.75\text{‰}$ )

SED

3, 591–613, 2011

## Dynamic magma mixing

O. Sigmarsson et al.

Title Page

Abstract

Introduction

Conclusions

References

Tables

Figures

◀

▶

◀

▶

Back

Close

Full Screen / Esc

Printer-friendly Version

Interactive Discussion



was used in the standard set. Day-to-day  $\delta^{18}\text{O}$  variability on the standards ranged from  $-0.1$  to  $+0.25$  ‰, and these values were added to the unknown samples to correct for day-to-day variability and absolute values on SMOW scale. The obtained precision on the standards is better than  $0.13$  ‰ and  $0.01$  ‰ in two sessions at 1 standard deviation.

### 4.2.3 Isotope ratios of Sr and Nd

About 100–150 mg of rock powder (chips for FH-3) were weighed into Teflon beakers for the samples and rock standards and leached for an hour in warm 6M HCl. After leaching the samples were washed in Milli-Q water and dissolved in a 2:1 mixture of concentrated  $\text{HNO}_3$  and HF on a hotplate for 3 days. After drying down the sample residue were redissolved in 6M HCl, dried down and redissolved again in 6M HCl, to obtain clear sample solutions. The samples for Sr and Nd analysis were dried down and redissolved in 1 M  $\text{HNO}_3$  and passed through TRU.Spec column chemistry, the Sr and Nd fractions was further purified through Sr. spec and LN. spec column chemistries, respectively (Pin et al., 1994, 1997).

The Sr samples were loaded onto single W-filaments and analysed at the Imperial College London MAGIC laboratories and Laboratoire Magmas et Volcans in Clermont-Ferrand on Triton TIMS in static mode. Rubidium interferences were monitored and corrected for, but were always lower than 40 ppm. Data were corrected for instrumental mass fractionation using the exponential law and  $^{88}\text{Sr}/^{86}\text{Sr} = 8.735209$ . Six analyses of NIST SRM 987 interspersed with the samples gave an average  $^{87}\text{Sr}/^{86}\text{Sr}$  value of  $0.710251 \pm 8$  ( $2\sigma$ ).

Neodymium was analyzed in static mode and data were corrected for instrumental mass fractionation using the exponential law and  $^{146}\text{Nd}/^{144}\text{Nd} = 0.7219$ , samples were analyzed in two analytical session during the first average value of the JNdi standard was  $^{143}\text{Nd}/^{144}\text{Nd} = 0.512099 \pm 20$ , during the second  $^{143}\text{Nd}/^{144}\text{Nd} = 0.512059 \pm 20$ . Sample data were normalized to  $^{143}\text{Nd}/^{144}\text{Nd}$  value of JNdi of 0.512113. Samarium

Title Page

Abstract

Introduction

Conclusions

References

Tables

Figures

◀

▶

◀

▶

Back

Close

Full Screen / Esc

Printer-friendly Version

Interactive Discussion



interferences were monitored and corrected for in run and lower than 100 ppm. The Nd procedural blank is 40 pg, no blank correction was made.

## 5 Results and discussion

Major-element concentrations show that the basalt of the flank eruption is mildly alkaline in composition (Table 1) similar to the magma erupted during the first half of the 1963–1967 Surtsey eruption 65 km south of Eyjafjallajökull (e.g. Jakobsson, 1979; Furman et al., 1991; Sigmarsson et al., 2009). Euhedral and normally zoned phenocrysts of olivines ( $Fo_{86-71}$ ) and plagioclases ( $An_{86-61}$ ) are abundant in addition to rare chromian spinel (inclusions in olivines) and clinopyroxene (Mg-number (100 x molar ratio of MgO over MgO + FeO) = 76–65). The magma is highly vesiculated and consequently the groundmass is largely crystallized (Fig. 2). The interstitial glass has evolved FeTi-basaltic composition similar to segregation veins at Surtsey and Holocene lavas from the Katla volcano (Sigmarsson et al., 2009; Oladottir et al., 2008). Less evolved basaltic compositions are preserved in melt inclusions of olivine and plagioclase phenocrysts (Moune et al., 2011). In contrast, bulk samples of tephra from the explosive phase of the 2010 Eyjafjallajökull eruption are of a benmoritic composition (Table 1). During the summit eruption, phenocryst compositions varied greatly with olivines ranging from  $Fo_{80}$  (Fig. 2) to  $Fo_{46}$ , feldspars vary from  $An_{69}$  to  $An_9$ , and Mg-number of clinopyroxene range from 72 down to 19. Magnetite is abundant and traces of apatite, pyrite and orthopyroxene are also present. Both the plagioclases and the clinopyroxenes display an inverse chemical zonation (e.g. Fig. 2e–f) with a core having, respectively, lower An content and Mg-number. Such compositional zonation is readily explained by magma mixing. Noteworthy are microsyenitic fragments composed of anorthoclase ( $An_{1.2}Or_{32}$ ), tridymite, ferrohedenbergite (Mg-number = 19;  $En_{11}Fs_{48}Wo_{41}$ ) and fluorite emitted during the first days of the summit eruption (Fig. 2d).

The major-element concentration variations for the whole-rock and glass analysis are shown in Fig. 3 where CaO vs MgO are plotted (a) and the molar ratios of CaO over  $Al_2O_3$  is displayed as function of the Mg-number (b). The whole-rock CaO/MgO

### Dynamic magma mixing

O. Sigmarsson et al.

Title Page

Abstract

Introduction

Conclusions

References

Tables

Figures

◀

▶

◀

▶

Back

Close

Full Screen / Esc

Printer-friendly Version

Interactive Discussion



decreased from 2.41 in the initial phase (sample EJ-1) to 1.48 in bread-crust bombs from the final stage of the eruption. Whole-rock sample of the first tephra (15 April) plots on a binary mixing line defined by the interstitial glass of the Fimmvörðuháls basalt and the glass composition of the 1821–1823 AD rhyolitic tephra. Three glass compositions are detected in the composite tephra from 17–19 April (sample EJ-2); basalt with SiO<sub>2</sub> of 49–51 %, benmorite (SiO<sub>2</sub> = 60–61 %) and trachyte (SiO<sub>2</sub> = 69–70 %; Fig. 3 and Table 2). These compositions plot on the same binary mixing line indicating mechanical mixing or mingling of the evolved basalts with older silicic melt. In-situ glass analyses of tephra produced between 22 April and 5 May (samples EJ-3,4,5) are all of intermediate composition. These tephra show increasingly lower whole-rock CaO/MgO values with time indicating changes in composition of mixing end-members during the eruption.

In-situ trace element measurements (see Table 3) in the three glass types of sample EJ-2, three glass inclusions in phenocrysts of the Fimmvörðuháls flank basalt, and in tephra glass from the 1821–1823 eruption confirm the role of mixing in forming the 2010 Eyjafjallajökull benmorite magma. Strong linear correlations are not only observed between incompatible element concentrations such as Rb and Th (Fig. 4), but also between those of compatible and incompatible elements (e.g. Sr versus Th.). This suggests that crystal-liquid separation had probably too little time to occur. The apparent absence of fractional crystallization despite tenfold variation in Th concentrations is best explained by rapid mechanical magma-mixing with minimal melt homogenisation prior to eruption. The whole-rock tephra trace element compositions (Table 1) plot on the same mixing line illustrating that despite changing composition of the mixing end-members during the eruption, they must have had similar Rb-Th and Sr-Th ratios. Uniform O, Sr and Nd isotope ratios in the whole rock lava and tephra samples (Table 1) support this conclusion. Delta <sup>18</sup>O of 5.8 ± 1 ‰ in EJ-1 is consistent with the silicic mixing end-member being formed by fractional crystallisation of mantle derived basalt similar to those erupted laterally on Fimmvörðuháls (δ<sup>18</sup>O = 5.4–5.8 ± 1 ‰). During this process the global partition coefficient of Sr (*D*<sub>Sr</sub>) between fractionating mineral assemblage and residual melt must have been close to unity (Fig. 4b).

**Dynamic magma mixing**

O. Sigmarsson et al.

Title Page

Abstract

Introduction

Conclusions

References

Tables

Figures

◀

▶

◀

▶

Back

Close

Full Screen / Esc

Printer-friendly Version

Interactive Discussion



**Dynamic magma  
mixing**

O. Sigmarsson et al.

Title Page

Abstract

Introduction

Conclusions

References

Tables

Figures

◀

▶

◀

▶

Back

Close

Full Screen / Esc

Printer-friendly Version

Interactive Discussion



The rapid magma mixing is also reflected in the highly heterogeneous and zoned mineral compositions in the benmoritic tephra. For instance, tephra that fell during the second peak in magma discharge (i.e. 5 and 6 May) contains 50  $\mu\text{m}$  zoned olivine (Fig. 2c) with 10  $\mu\text{m}$  thick rim having a composition of  $\text{Fo}_{48-50}$ , but a core of  $\text{Fo}_{80}$  indistinguishable from olivines in the Fimmvörðuháls basalts. This suggests arrival of deep-derived primitive basalts that is consistent with a deep seismic swarm (originating from a depth close to the mantle-crust boundary (Hjaltadóttir et al., 2011; Bjarnason, 2008)) and increased magma output as observed by higher eruption column on 5 May. The new influx of more primitive basalt magma coincides with changes in the composition of the silicic mixing end-member changing to a less evolved composition as indicated by the mixing curves and lines on Fig. 3. The composition of the final mixing end-member is present in the EJ-5 tephra and identified as low temperature melting component of a Na-rich plagioclase (Fig. 2e–f). This suggests that the stagnant residual melt from the 1821–1823 eruption was somewhat consumed by mixing with basalts by 5 May, after which the magma chamber's carapace (Fig. 1d) was partially melted by interaction with newly injected and hotter mantle-derived basalts. Taken together, the explosive Eyjafjallajökull eruption is best explained by dynamic mixing involving older silicic intrusion that was heated up and remobilized by the injection of hot basalt magma that became more primitive with time.

The high resolution sample suite from the 2010 Eyjafjallajökull eruption allow us to estimate a) the proportions of the basalt component in the mixed magma and its variations with time, and b) the time-dependent changes in the composition of the deep-derived basalt magma (Fig. 4). These estimates are obtained from the calculated binary mixing curves shown in Fig. 3b, and from the intercept of the mixing lines with the fractional crystallisation vector of the basalts applying the lever rule (see legend to Fig. 3). The results indicate that the proportions of the basalt decreased from approximately 50 % late April to less than 30 % a month later whereas the evolved FeTi-basalt composition early in the eruption was progressively replaced by more primitive basalt composition at the end.



of the present study clearly underline how fast magma mixing components can change.

## 6 Conclusions

The explosive summit eruption of Eyjafjallajökull in 2010 was triggered by an injection of Mg-rich basaltic magma several months earlier. That basalt stagnated below a silicic magma body, presumably residues from the penultimate rhyolitic eruption in 1821–1823, degassed, partially crystallized and evolved to a FeTi-basalt. The heat and gas liberated rose up into the half-frozen silicic magma opening a pathway for the evolved basalt that triggered the explosive eruption on 14 April through magma mingling within the silicic reservoir. In the meantime, the Mg-rich magma by-passed the central magma chamber and produced a flank eruption until the passage through the central conduit opened up. Early May, the evolved basalt was consumed by the magma mingling and deeper Mg-rich basalt rose from a depth in excess of 20 km into the silicic reservoir and caused increased magma output and corresponding higher eruption column. The additional heat brought in by the fresh intrusion caused partial melting of the microgranitic carapace causing compositional changes in the mixing end-members. Finally, the basalt injection declined and the eruption came to a halt.

*Acknowledgements.* Sigurdur R. Gislason collected sample EJ-1. Analytical assistance by Chantal Bosq, Delphine Auclair-Aubierge and Mahmmmed Benbakkar was much appreciated. Funding from the Icelandic government is acknowledged.

## References

- Barclay, J., Herd, R. A., Edwards, B. R., Christopher, T., Kiddle, E. J., Plail, M., and Donovan, A.: Caught in the act: implications for the increasing abundance of mafic enclaves during the recent eruptive episodes of the Soufrière Hills volcano, Montserrat., *Geophys. Res. Lett.*, 37, L00E09, doi:10.1029/2010GL042509, 2010.
- Bjarnason, I. Th.: An Iceland hotspot saga: Jökull, 58, 3–16, 2008.

SED

3, 591–613, 2011

## Dynamic magma mixing

O. Sigmarsson et al.

Title Page

Abstract

Introduction

Conclusions

References

Tables

Figures

◀

▶

◀

▶

Back

Close

Full Screen / Esc

Printer-friendly Version

Interactive Discussion



**Dynamic magma mixing**

O. Sigmarsson et al.

Title Page

Abstract

Introduction

Conclusions

References

Tables

Figures

◀

▶

◀

▶

Back

Close

Full Screen / Esc

Printer-friendly Version

Interactive Discussion



- Eichelberger, J. C.: Vesiculation of mafic magma during replenishment of silicic magma reservoirs: *Nature*, 288, 446–450, 1980.
- Fabbrizio, A., Schmidt, M. W., Günther, D., and Eikenberg, J.: Experimental determination of Ra mineral/melt partitioning for feldspars and  $^{226}\text{Ra}$ -disequilibrium crystallization ages of plagioclase and alkali-feldspar, *Earth Planet. Sci. Lett.*, 280, 137–148, 2009.
- Furman, T., Frey, F. A., and Park, K.-H.: Chemical constraints on the petrogenesis of mildly alkaline lavas from Vestmannaeyjar, Iceland: the Eldfell (1973) and Surtsey (1963–1967) eruptions, *Contribution to Mineralogy and Petrology*, 109, 19–37, 1991.
- Gudmundsson, M. T., Pedersen, R., Vogfjörd, K., Thorbjarnardottir, B., Jakobsdottir, S., and Roberts, M.: Eruptions of Eyjafjallajökull Volcano, Iceland, *Eos*, 91, 190–191, 2010.
- Hjaltadottir, S., Vogfjörd, K., and Slunga, R.: A Seismological Image of the Eyjafjallajökull Plumbing System during 2009–2010. *Geophysical Research Abstracts Vol. 13*, EGU2011–12221, 2011.
- Jakobsson, S. P.: Petrology of Recent basalts from the Eastern Volcanic Zone, Iceland, *Acta Naturalia Islandica*, 26, 1–103, 1979.
- Jarosewich, E., Nelen, J. A., and Borberg, J. A.: Electron microprobe reference samples for mineral analysis, in: *Smithsonian Institution Contributions to the Earth Sciences No. 22*, edited by: Fudali, R. F., Smithsonian Institution Press, 68–72, 1979.
- Martin, E. and Sigmarsson, O.: Geographical variations of silicic magma origin in Iceland: the case of Torfajökull, Ljósufjöll and Snæfellsjökull volcanoes, *Contribution to Mineralogy and Petrology*, 153, 593–605, 2007.
- Moune, S., Sigmarsson, O., Schiano, P., Thordarson, Th., and Hayward, C.: Volatile characterisations of Eyjafjallajökull volcano (Iceland): from the magmatic source at depth to the surface. *Geophysical Research Abstracts Vol. 13*, EGU2011–4184, 2011.
- Nakamura, M.: Continuous mixing of crystal mush and replenished magma in the ongoing Unzen eruption, *Geology*, 23, 807–810, 1995.
- Oladottir, B., Sigmarsson, O., Larsen, G., and Thordarson, Th.: Temporal evolution of the magma plumbing system beneath Katla volcano Iceland, *B. Volcanol.*, 70, 475–493, 2008.
- Pallister, J. S., Thornber, C. R., Cashman, K. V., Clynne, M. A., Lowers, H. A., Mandeville, C. W., Brownfield, I. K., and Meeker, G. P.: Petrology of the 2004–2006 Mount St. Helens lava dome – Implications for magmatic plumbing and eruption triggering, in: *A volcano rekindled; the renewed eruption of Mount St. Helens, 2004-2006*, edited by: Sherrod, D. R., Scott, W. E., and Stauffer, P. H., U.S. Geological Survey Professional Paper 1750, 647–702, 2008.



Dynamic magma  
mixing

O. Sigmarsson et al.

**Table 1.** Whole-rock major- and trace-element concentrations and Sr-, Nd- and O-isotope ratios in Eyjafjallajökull 2010 products.

Sample #	FH-1	FH-2	FH-3	FH-4	EJ-1	EJ-3	EJ-4	EJ-5	EJ-6	EJ-7	EJ-5'	EJ-6'	EJ-7'	BHVO-1	BHVO-1'	BHVO-1 certified values
SiO <sub>2</sub>	46.3	46.29	46.81	45.93	56.62	55.28	55.05	57.81	61.26	57.57	57.24	61.44	57.58	49.3	49.39	49.94
TiO <sub>2</sub>	2.99	3.05	2.90	2.73	1.72	1.77	1.8	1.52	1.17	1.58	1.5	1.12	1.49	2.68	2.69	2.71
Al <sub>2</sub> O <sub>3</sub>	14.95	15.12	15.09	14.88	14.95	14.74	15.02	14.97	14.56	14.61	14.95	14.89	14.87	13.9	14.02	13.8
Fe <sub>2</sub> O <sub>3-t</sub>	13.85	13.69	13.01	13.12	10.65	10.85	10.8	10.33	8.21	10.05	10.15	8.22	9.98	12.32	12.36	12.23
MnO	0.19	0.18	0.18	0.18	0.24	0.23	0.24	0.24	0.2	0.23	0.23	0.19	0.22	0.17	0.17	0.17
MgO	8.77	8.21	8.50	9.05	2.23	3.6	2.95	3.2	2.3	3.56	3.21	2.21	3.43	7.16	7.2	7.23
CaO	9.9	10.03	10.28	9.89	5.37	5.89	5.95	5.33	4.02	5.27	5.38	4.11	5.23	11.62	11.5	11.4
Na <sub>2</sub> O	2.73	2.74	2.97	3.14	5.24	5.31	5.86	5.33	5.77	5.19	5.35	5.61	5.24	2.29	2.48	2.26
K <sub>2</sub> O	0.63	0.56	0.67	0.59	1.74	1.59	1.61	1.81	2.56	1.86	1.81	2.33	1.82	0.51	0.51	0.52
P <sub>2</sub> O <sub>5</sub>	0.4	0.41	0.42	0.39	0.48	0.38	0.39	0.34	0.21	0.34	0.33	0.2	0.31	0.26	0.26	0.27
H <sub>2</sub> O+	0.04	0.08	0.17	0.15	0.58	0.18	0	0.03	0.01	0.03	-0.03	0.01	0.03	0.16	0.16	0.16
H <sub>2</sub> O-	-0.85	-0.89	-0.84	-0.78	0.03	0.19	0	-0.3	-0.27	-0.47	-0.3	-0.27	-0.47	0.05	0.05	0.05
Total	99.96	99.55	100.16	99.33	99.92	100.08	99.74	100.67	100.07	99.88	99.9	100.13	99.82	100.47	100.86	100.8
Rb	12.0		12.8	11.9	38.8	36.1	35.3	41.1	54.9	41.9						
Sr	452		456	458	346	342	355	313	217	299						
Th	1.69		1.81	1.71	5.62	5.16	5.04	5.91	7.93	6.09						
U	0.535		0.564	0.538	1.73	1.61	1.56	1.83	2.45	1.86						
<sup>87</sup> Sr/ <sup>86</sup> Sr	0.703259		0.703254		0.703257	0.703246		0.703241								
2SE	0.000006		0.000007		0.000008	0.000007		0.000008								
<sup>143</sup> Nd/ <sup>144</sup> Nd	0.512998		0.512985		0.513004	0.513000		0.513003								
2SE	0.000005		0.000003		0.000006	0.000005		0.000004								
δ <sup>18</sup> O ‰	5.83		5.43		5.96	5.58			5.48							
sd	0.19		0.24		0.18	0.20			0.02							

Major- and trace-element concentrations are given in wt %, and ppm, respectively. Abbreviations SE and sd denote standard error and standard deviation, respectively. Apostrophes behind a sample number denote a replicate analysis.

Title Page

Abstract

Introduction

Conclusions

References

Tables

Figures

◀

▶

◀

▶

Back

Close

Full Screen / Esc

Printer-friendly Version

Interactive Discussion



**Table 2.** Electron probe microanalysis of glasses in Eyjafjallajökull's tephra.

	SiO <sub>2</sub>	TiO <sub>2</sub>	Al <sub>2</sub> O <sub>3</sub>	FeO	MnO	MgO	CaO	Na <sub>2</sub> O	K <sub>2</sub> O	P <sub>2</sub> O <sub>5</sub>	Total	
EJ-1-1	59.64	1.38	14.93	8.36	0.29	1.38	4.00	5.44	2.33	0.49	98.26	
EJ-1-2	65.87	0.51	16.55	3.52	0.10	0.26	2.55	6.21	2.37	0.60	98.54	
EJ-2-1	50.41	3.88	12.65	13.70	0.25	3.78	8.01	3.47	1.33	0.81	98.27	
EJ-2-2	50.22	3.71	12.77	13.58	0.26	4.11	8.49	3.40	1.17	0.82	98.52	
EJ-2-3	51.23	3.95	12.59	14.29	0.24	3.52	7.71	3.08	1.53	1.09	99.23	
EJ-2-4	51.48	3.85	12.54	14.33	0.21	3.57	7.66	3.26	1.55	1.00	99.43	
EJ-2-5	51.35	3.90	12.56	14.31	0.23	3.54	7.68	3.17	1.54	1.05	99.33	
EJ-2-7	68.35	0.34	13.94	4.29	0.09	0.12	1.06	5.30	3.69	0.04	97.24	
EJ-2-8	70.11	0.33	13.36	3.31	0.22	0.02	0.27	5.59	4.61	0.00	97.83	
EJ-2-9	59.07	1.59	14.85	8.75	0.24	1.47	4.00	5.14	2.40	0.54	98.03	Benmorite
EJ-2-11	60.09	1.47	14.74	8.51	0.33	1.49	3.89	5.08	2.51	0.40	98.51	to
EJ-3-1	57.80	2.08	14.80	9.38	0.23	2.04	4.93	4.90	2.18	0.48	98.82	trachyte
EJ-3-2L	57.63	2.02	14.77	9.78	0.21	2.00	4.88	4.23	2.24	0.46	98.23	
EJ-3-2D	60.49	1.75	14.24	9.15	0.29	1.52	3.89	3.93	2.63	0.64	98.54	
EJ-4	58.26	2.09	14.00	9.71	0.24	2.03	4.66	4.46	2.37	0.49	98.30	
EJ-5-1.1	63.59	1.26	14.09	8.17	0.17	1.03	2.79	3.34	3.09	0.47	98.00	
EJ-5-2.2	62.28	1.42	14.17	8.12	0.34	1.25	3.08	3.25	2.93	0.40	97.23	
EJ-5-2.3	62.77	1.25	14.57	7.82	0.30	1.16	3.09	3.97	3.05	0.43	98.42	
EJ-5-4.1	60.96	1.69	14.36	8.20	0.24	0.58	2.26	4.75	2.12	0.40	95.58	
EJ-5-4.2	57.29	1.66	16.01	10.13	0.24	1.60	4.44	4.95	2.73	0.28	99.31	
EJ-5-4.4	58.83	1.62	16.40	10.04	0.13	0.97	2.46	5.38	3.81	0.37	100.02	
EJ-5-4.5	57.52	1.55	15.92	10.12	0.20	1.94	5.14	3.93	3.03	0.37	99.73	
EJ-5-10.1	61.76	1.49	14.45	8.20	0.14	1.37	3.28	4.30	2.88	0.44	98.30	
EJ-5-10.2	62.33	1.41	14.79	6.38	0.20	1.17	3.50	4.62	3.07	0.36	97.84	
EJ-5-11.1	61.77	1.36	13.80	7.55	0.30	1.19	3.15	4.56	4.02	0.45	98.16	
EJ-5-11.2	61.77	1.34	14.04	8.19	0.42	1.17	3.28	4.71	3.97	0.61	99.51	
EJ-5-11.3	61.09	1.36	14.03	8.14	0.34	1.19	3.12	4.70	4.03	0.43	98.43	
EJ-5-14.1	58.34	2.71	13.46	11.86	0.35	1.53	3.47	5.96	1.82	0.40	99.90	
EJ-5-14.2	60.93	1.43	14.02	8.12	0.27	1.36	3.33	4.66	2.92	0.46	97.51	
EJ-5-15.1	62.60	1.41	14.18	8.37	0.18	1.25	3.15	4.85	3.01	0.43	99.43	
EJ-5-15.2	64.58	1.00	15.88	6.19	0.23	0.77	2.70	4.21	2.68	0.39	98.64	
FH-glass	46.83	4.80	13.15	14.44	0.22	4.62	9.60	3.28	1.00	0.71	98.65	Average of 35 analysis
MI Fo>86	46.41	3.58	14.79	11.89	0.16	5.93	10.06	3.33	0.71	0.47	97.33	Average of 5 analysis
MI Plag	46.33	3.33	14.12	12.15	0.22	5.78	9.71	3.48	0.86	0.42	96.39	Average of 3 analysis
Katla	47.21	4.73	12.87	14.83	0.24	4.78	9.54	3.04	0.78	0.71	98.73	Average of historical tephra
EJ-1821	60.63	1.58	14.54	8.72	0.26	1.30	3.40	4.50	3.06	0.42	98.42	Average of 7 grains

Title Page

Abstract

Introduction

Conclusions

References

Tables

Figures



Back

Close

Full Screen / Esc

Printer-friendly Version

Interactive Discussion





## Dynamic magma mixing

O. Sigmarsson et al.

Title Page

Abstract

Introduction

Conclusions

References

Tables

Figures

◀

▶

◀

▶

Back

Close

Full Screen / Esc

Printer-friendly Version

Interactive Discussion



Table 3. Continued.

	EJ-2		A-THO		NIST610										Mean	SD
	Grain9	Grain11	I	II	I	II	III	IV	V	VI	VII	VIII	IX			
Li	13.5	18.6	28.9	28.9	465	468	456	468	461	467	469	468	467	465	4.11	
Sc	10.4	14.7	7.48	8.79	449	448	441	455	452	455	449	450	451	450	4.22	
V	31.1	35.6	2.53	3.24	445	444	439	450	452	448	455	454	461	450	6.84	
Rb	40.6	53.3	63.3	63.7	424	428	422	422	417	418	426	430	430	424	4.74	
Sr	339	201	86.6	89.1	493	489	487	491	489	490	496	490	492	491	2.46	
Y	48.3	65.6	87.1	87.0	445	442	444	448	447	448	447	445	448	446	2.25	
Zr	387	517	443	455	418	416	413	415	410	413	409	408	405	412	4.17	
Nb	56.0	73.0	53.5	53.7	455	459	453	452	449	456	456	454	452	454	2.89	
Ba	421	457	507	518	419	420	421	421	424	425	433	431	437	426	6.43	
La	46.7	59.0	52.7	53.1	427	426	423	428	425	429	429	429	432	428	2.76	
Ce	104	133	118	119	437	439	437	443	444	447	456	452	450	445	6.74	
Pr	12.2	16.2	14.0	13.8	429	427	428	432	435	434	440	437	442	434	5.18	
Nd	48.3	68.4	57.5	59.9	433	434	427	416	409	413	415	411	411	419	9.71	
Sm	11.1	15.0	13.1	12.3	439	434	439	437	436	433	440	442	444	438	3.60	
Eu	4.03	4.26	2.47	2.97	417	416	415	423	419	421	436	431	434	424	7.95	
Gd	10.1	14.8	14.5	14.5	416	416	412	429	425	424	444	443	447	428	13.42	
Tb	1.56	2.13	2.25	2.18	405	404	400	414	407	413	423	421	420	412	8.23	
Dy	9.32	12.9	15.2	15.9	433	420	417	427	427	425	431	438	433	428	6.64	
Ho	1.82	2.67	3.1	3.26	437	435	430	445	439	435	449	438	444	439	5.97	
Er	5.02	7.05	10.3	10.2	430	433	428	441	438	438	443	442	443	437	5.59	
Tm	0.699	1.09	1.38	1.39	427	429	426	434	437	432	441	440	440	434	5.73	
Yb	4.16	6.86	9.97	10.1	456	456	444	459	455	459	464	467	462	458	6.44	
Lu	0.793	1.09	1.55	1.29	431	433	429	440	441	436	443	444	443	438	5.81	
Hf	8.53	12.1	12.9	12.1	389	393	388	396	402	400	406	406	405	398	7.06	
Ta	3.6	4.5	3.92	3.47	467	468	458	467	460	469	461	463	462	464	3.93	
Pb	4.77	5.81	5.99	5.87	429	425	420	427	423	430	437	437	435	429	6.02	
Th	4.98	6.59	6.87	7.24	437	440	437	442	445	443	447	450	448	443	4.81	
U	1.58	2.2	2.01	2.05	436	441	442	450	447	450	457	459	461	449	8.57	

The first two MI in olivine with Fo73 and the two A-THO analysis are duplicate analysis of the same glass patch. The standard glass NIST610 was run as an unknown during different runs and yields the overall reproducibility.

**Dynamic magma mixing**

O. Sigmarsson et al.

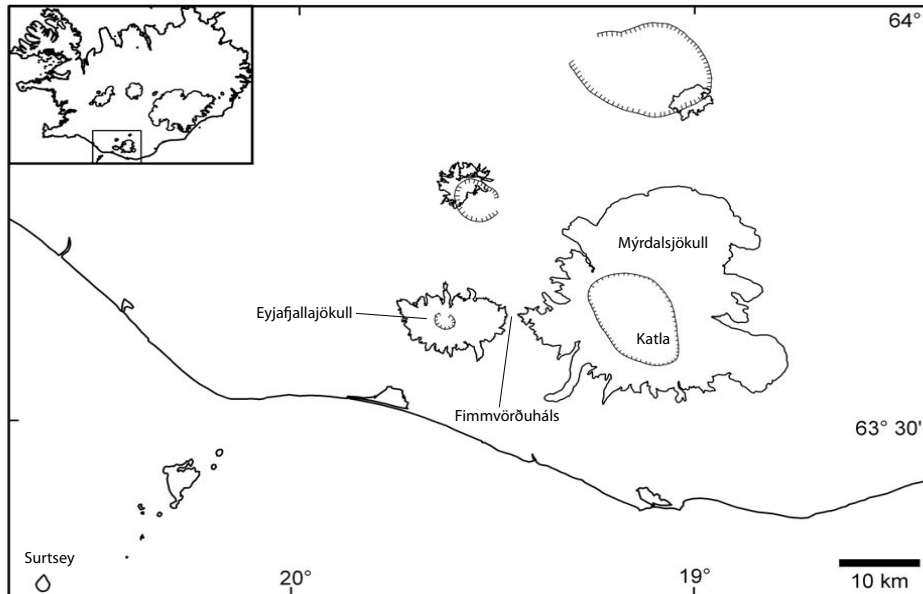


**Fig. 1.** Location of Eyjafjallajökull and Mýrdalsjökull ice-caps, the latter of which covers the Katla volcano. The pass between the two ice-caps, Fimmvörðuháls, was the location of the basaltic flank eruption preceding the summit eruption of Eyjafjallajökull in 2010.

Title Page

Abstract

Introduction

Conclusions

References

Tables

Figures

◀

▶

◀

▶

Back

Close

Full Screen / Esc

Printer-friendly Version

Interactive Discussion



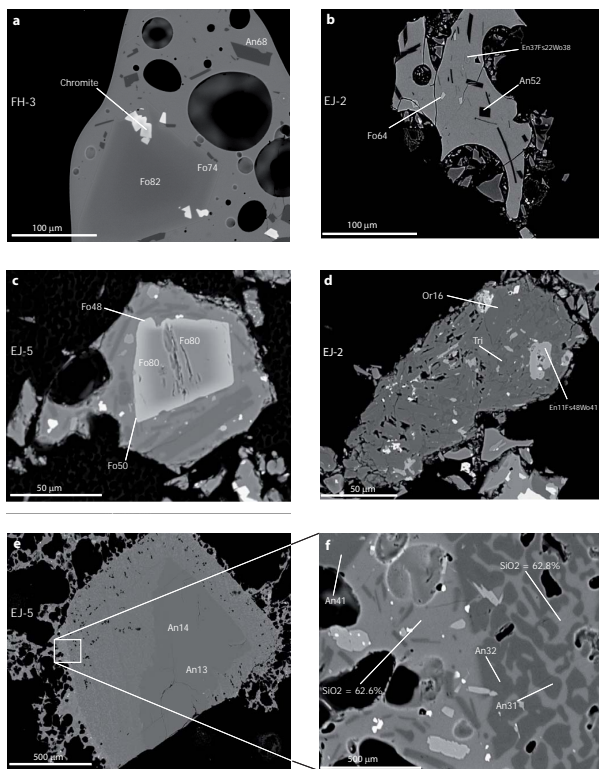


**Fig. 2.** Backscattered-electron images of individual tephra grains from the 2010 Eyjafjallajökull eruption: **(a)** high-MgO basalt produced 1 April during the flank eruption at Fimmvörðuháls **(b)** evolved basalt emitted together with tephra of silicic and intermediate composition during the early (17–19 April) explosive phase (note the bent plagioclase lath that grew contemporaneously with the large vesicle illustrating gas exsolution driven crystallisation); **(c)** cracked Mg-rich olivine-core mantled with iron-richer olivine set in partly crystalline groundmass from 5 May; it is indicative of injection of primitive basalt into the silicic magma body; **(d)** microsyenitic fragment composed of alkali feldspar, sodic plagioclase, ferroshedenbergite, tridymite and fluorite minerals; **(e–f)** destabilised oligoclase that upon melting yielded trachytic melt and calcium-richer plagioclase. Sample numbers are given at the left boundary of each image.

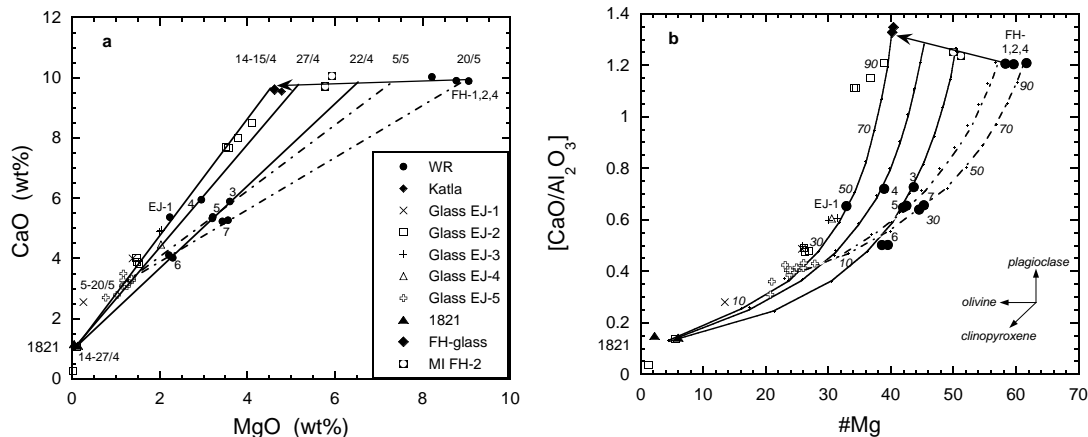


**Fig. 3.** Major-element variations in 2010 Eyjafjallajökull tephra and lava. **(a)** CaO versus MgO showing a near-horizontal fractionation vector from Fimmvörðuháls whole-rock basalt compositions (samples with prefix FH) to that of the corresponding interstitial glasses and Katla 1918 basalt glasses (Oladottir et al., 2008). Mixing lines between these evolved basalt compositions and the two silicic end-members, the 1821–1823 rhyolite and oligoclase melt of 5 May (dash-dot line) are also shown. The intercepts of these lines with the basaltic fractionation vector is used to estimate the degree of basaltic evolution (expressed as mixing proportions between evolved and primitive basalts in Fig. 5) in the mafic mixing pole. Dates of samples corresponding to different intercepts are shown in addition to the interval of active silicic mixing poles. **(b)** Molar ratios of CaO over  $Al_2O_3$  against the Mg-number (#Mg = molar MgO over the sum of MgO plus FeO calculated from total iron analysed by assuming  $Fe_2O_3/FeO$  of 0.2). In the lower right corner are shown schematically the melt composition vectors of pure mineral fractionation from basalt. These are consistent with olivine domination on the fractionation vector from FH-basalt, but the trend of EJ-2 basalt glasses indicates clinopyroxene fractionation. Binary mixing curves are calculated using the same end-member composition as in a). Mixing proportions of basalt to silicic melt are derived from the calculated curves. Duplicate analyses of three Eyjafjallajökull bulk-tephra (EJ-5, 6, 7) indicate the overall analytical precision. Abbreviations are WR for whole-rock compositions, EJ for Eyjafjallajökull, FH for Fimmvörðuháls flank basalts and MI for melt inclusions.

[Title Page](#)
[Abstract](#)
[Introduction](#)
[Conclusions](#)
[References](#)
[Tables](#)
[Figures](#)
[◀](#)
[▶](#)
[◀](#)
[▶](#)
[Back](#)
[Close](#)
[Full Screen / Esc](#)
[Printer-friendly Version](#)
[Interactive Discussion](#)


## Dynamic magma mixing

O. Sigmarsson et al.

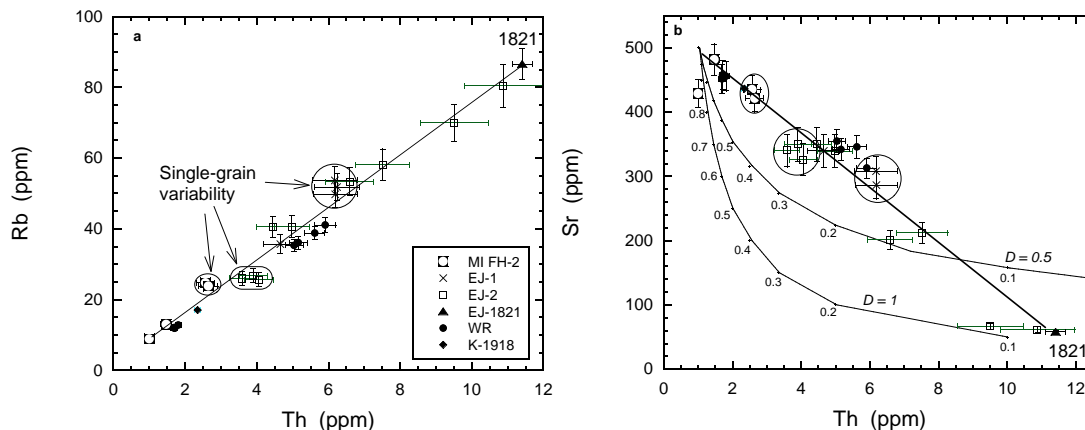


**Fig. 4.** Linear correlations of Rb, Sr, and Th concentrations between extreme magma compositions produced during the 2010 Eyjafjallajökull eruption. Four spot analyses of three olivine-hosted melt inclusions are shown for comparison. Larger error bars for the in-situ analysis, compared to those of whole-rock (WR), are caused by small ablation crater-size (diameter of 11  $\mu\text{m}$ ), due to small area of crystal-free glass patches, and consequent lower count rates of each element. Multiple analyses of single grains are encircled in both panels. In (b), two curves of melt evolution during hypothetical crystal fractionation are shown for different  $D_{Sr}$  (assuming  $D_{Th}$  close to 0) with the remaining melt fractions indicated. The origin of the 1821–1823 alkaline rhyolite will be addressed elsewhere but it is consistent with over 90% fractional crystallisation from primitive basalt. This differentiation mechanism appears dominant at Icelandic volcanoes close to the periphery of the island (Martin and Sigmarsson, 2007). Apatite fractionation, which  $D_{Sr}$  can be as high as 5 (Prowatke and Klemme, 2006), together with that of plagioclase, having  $D_{Sr}$  in the range 1–3 (Fabbrizio et al., 2009), account for a global  $D_{Sr}$  as high as unity.

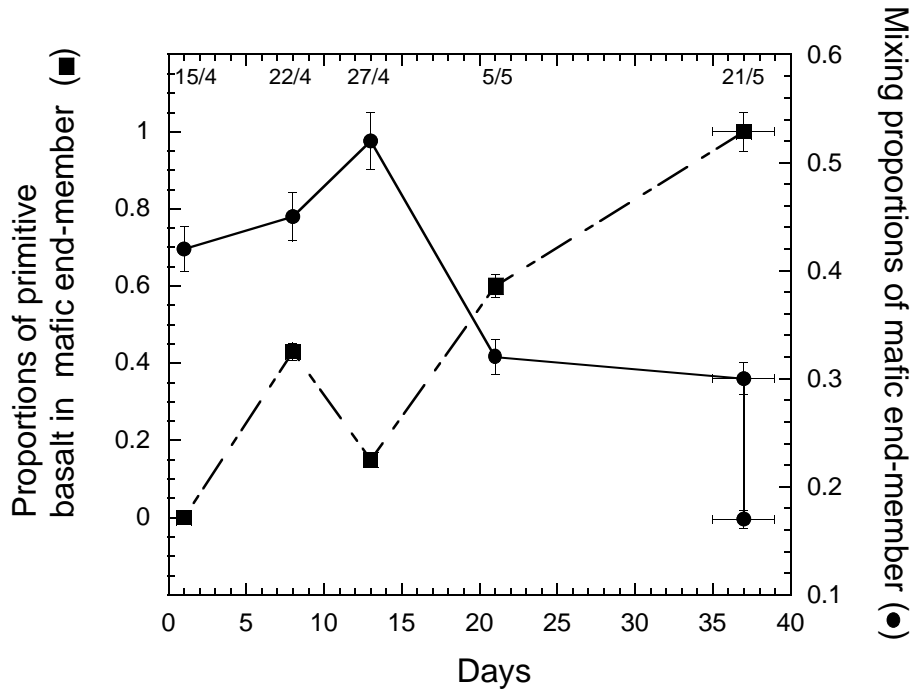


**Fig. 5.** Mixing proportions as a function of time of primitive basalt in the mafic end-member (scale on left y-axis) and that of basalt melt in the benmoritic tephra of Eyjafjallajökull. Arbitrary 5% error is assigned to the estimated magma mixing proportions that are derived from Fig. 3. The decrease of the basalt component suggests that supply of silicic magma at depth is abundant (see text for further details).

Title Page

Abstract

Introduction

Conclusions

References

Tables

Figures

◀

▶

◀

▶

Back

Close

Full Screen / Esc

Printer-friendly Version

Interactive Discussion

